Theoretical criteria for scattering dark states in nanostructured particles

Chia Wei Hsu,[*,†,‡] Brendan G. DeLacy,[¶] Steven G. Johnson,[§] John D. Joannopoulos,[†] and Marin Soljačić[†]

Department of Physics, Massachusetts Institute of Technology, Cambridge, MA 02139, USA., Department of Physics, Harvard University, Cambridge, MA 02138, USA., U.S. Army Edgewood Chemical Biological Center, Aberdeen Proving Ground, MD 21010, USA., and Department of Mathematics, Massachusetts Institute of Technology, Cambridge, MA 02139, USA.

E-mail: cwhsu@mit.edu

[*]To whom correspondence should be addressed
[†]Department of Physics, Massachusetts Institute of Technology, Cambridge, MA 02139, USA.
[‡]Department of Physics, Harvard University, Cambridge, MA 02138, USA.
[¶]U.S. Army Edgewood Chemical Biological Center, Aberdeen Proving Ground, MD 21010, USA.
[§]Department of Mathematics, Massachusetts Institute of Technology, Cambridge, MA 02139, USA.

Abstract

Nanostructures with multiple resonances can exhibit a suppressed or even completely eliminated scattering of light, called a scattering dark state. We describe this phenomenon with a general treatment of light scattering from a multi-resonant nanostructure that is spherical or non-spherical but subwavelength in size. With multiple resonances in the same channel (*i.e.* same angular momentum and polarization), coherent interference always leads to scattering dark states in the low-absorption limit, regardless of the system details. The coupling between resonances is inevitable and can be interpreted as arising from far-field or near-field. This is a realization of coupled-resonator-induced transparency in the context of light scattering, which is related to but different from Fano resonances. Explicit examples are given to illustrate these concepts.

KEYWORDS: Scattering dark states, nanostructures, light scattering, coupled-resonator-induced transparency, Fano resonances, temporal coupled-mode theory

When macroscopic structures are shrunk to the nanoscale, their optical properties depart dramatically from the intuitive ray-optics picture.[1] Subwavelength structures on resonance can have scattering cross sections much larger than their geometrical sizes,[2,3] and the presence of multiple resonances leads to even more possibilities through mode hybridization[4] and interference effects.[5–9] A particularly interesting phenomenon is the suppressed scattering in nanostructures with multiple plasmonic resonances,[10–23] plasmonic and excitonic resonances,[24–30] or dielectric resonances,[31,32] referred to collectively as a "scattering dark state." A wealth of models has been employed to describe this suppressed scattering, ranging from perturbative models,[12] generalization of the Fano formula,[13–15] and electrostatic approximation,[22,23] to coupled-mechanical-oscillator models.[17–21] These models reveal valuable insights and facilitate the design of specific structures with desired line shapes. However, the general criteria for observing such scattering dark states remain unclear. Non-scattering states have been known in atomic physics since the early works of Fano[33] and have been discovered in a variety of nanoscale systems in recent years[5–8,34,35]. However, Fano resonances generally concern the interference between a narrow discrete resonance and a broad resonance or continuum. Meanwhile, many occurrences of the scattering dark state involve the interference between multiple narrow discrete resonances, and it seems necessary to treat the multiple resonances at equal footing. Thus, we seek a formalism analogous to the phenomenon of coupled-resonator-induced transparency[5] that has been established in certain other systems such as coupled mechanical oscillators[36,37], coupled cavities[38,39], coupled microring resonators[40–44], and planar metamaterials[45–48].

Here, we derive the general equations governing the resonant light scattering from a spherical or a non-spherical but subwavelength obstacle, accounting for multiple resonances with low loss. Due to the spherical symmetry (or the small size) of the obstacle, different channels of the multipole fields are decoupled. We find that within each channel, n resonances always lead to $n-1$ scattering dark states in the low-absorption limit. This universal result is independent of the radiative decay rates of the resonances, method of coupling (can be

near-field or far-field), nature of the resonances (can be plasmon, exciton, whispering-gallery, *etc.*), number of resonances, which of the multipole, TE or TM polarization, and other system details. With different choices of basis, one can interpret the scattering dark state as arising from the far-field coupling of multiple radiating resonances, or arising from the near-field coupling of a radiating and several non-radiating resonances. We provide explicit examples using plasmonic resonances and whispering-gallery resonances, showing zero scattering for lossless materials and significantly suppressed scattering for realistic materials with loss. We also discuss potential applications for slow light, transparent projection screen, and wavelength-selective transmission.

Consider a linearly polarized planewave incident on an obstacle that is spherical or non-spherical but much smaller than the wavelength of the incident light. This obstacle can have arbitrary number of layers and material composition; in the small-obstacle case, it can also be a cluster of particles. We start with the general formalism for such a scattering problem. Outside the obstacle, the electric field can be written as $\mathbf{E} = \nabla\times(\mathbf{r}\psi_{\mathrm{TE}}) - (i/k)\nabla\times\nabla\times(\mathbf{r}\psi_{\mathrm{TM}})$, where $\mathbf{r}$ is position from the particle center, k is the wave number, and ψ_σ is a scalar function satisfying the Helmholtz equation.[1] We use σ to denote the two polarizations: transverse-electric (TE) or transverse-magnetic (TM), where the electric or magnetic field is perpendicular to $\mathbf{r}$. Choose our coordinate such that the x axis and the z axis is aligned with the polarization and the propagation direction of the incident light respectively. The incident planewave consists of all multipole terms with $l > 0$ and $m = 1$ in both TE and TM[1], so the general solution can be written as

$$\psi_\sigma(r,\theta,\phi) = f_\sigma(\phi)\sum_{l=1}^{\infty}\left[s^-_{l,\sigma}h^{(1)}_l(kr) + s^+_{l,\sigma}h^{(2)}_l(kr)\right]P^1_l(\cos\theta), \tag{1}$$

where $f_{\mathrm{TE}}(\phi) = \sin\phi$, $f_{\mathrm{TM}}(\phi) = \cos\phi$, $h^{(1)}_l$ (or $h^{(2)}_l$) is the spherical Henkel function of the first (or second) kind corresponding to outgoing (or incoming) spherical wave, and P^1_l is the associated Legendre polynomial with $m = 1$. The amplitudes of outgoing and incoming waves

$s^{\mp}_{l,\sigma}$ are coefficients of the general solution. Here, each angular momentum and polarization pair (l,σ) corresponds to a distinct "channel." The spherical symmetry (or the small size) of the obstacle means that different channels are decoupled, so optical response properties are given by the reflection coefficients $R_{l,\sigma} \equiv s^{-}_{l,\sigma}/s^{+}_{l,\sigma}$. Energy conservation requires that $|R_{l,\sigma}| \leq 1$ in each channel. The total scattering cross section of this particle is given by

$$\sigma_{\text{sca}} = \frac{\lambda_{\text{m}}^2}{8\pi} \sum_{\sigma} \sum_{l=1}^{\infty} (2l+1) \left|1 - R_{l,\sigma}\right|^2 , \tag{2}$$

where λ_{m} is the wavelength in the surrounding medium. Note that there is no inter-channel interference here, unlike the intensity of the scattered light at a specific angle (such as back scattering) where different channels of spherical waves can interfere[6,49].

In each channel, the scattering from a single low-loss resonance is given by a Lorentzian function[2,3,34,35]. Therefore, when we consider multiple resonances each in a different channel, the total response will be a sum of Lorentzians with no scattering dark state; this is illustrated schematically in Figure 1a. For a scattering dark state, we need multiple overlapping resonances in the same channel, as illustrated in Figures 1b and 1c.

We start with the simplest case of two resonances in channel (l,σ), as illustrated in Figure 2a. The two resonances may be of any nature (*e.g.*, plasmon, exciton, whispering-gallery). When the resonances have low loss, $R_{l,\sigma}$ has two poles on the complex-frequency plane, near which the system follows a simple set of equations described by the temporal coupled-mode theory (TCMT).[2,34,35,39,50] As a starting point, we "turn off" the radiation loss and absorption loss of the resonances, and the resonance amplitudes A'_j $(j = 1, 2)$ evolve as

$$\frac{d}{dt} \begin{pmatrix} A'_1 \\ A'_2 \end{pmatrix} = -i \begin{pmatrix} \omega'_1 & \omega'_{12} \\ \omega'_{21} & \omega'_2 \end{pmatrix} \begin{pmatrix} A'_1 \\ A'_2 \end{pmatrix} , \tag{3}$$

where ω'_j are the resonant frequencies, and ω'_{12}, ω'_{21} are the near-field coupling strengths. We proceed by changing to the basis A_j (without the primes) that diagonalizes the matrix

(so ω_{12} is now zero), which is always possible because the matrix is Hermitian by energy conservation. In the new basis, we "turn on" the low losses of the resonances, and couple them to the spherical wave in channel (l, σ),

$$\frac{d}{dt}\begin{pmatrix} A_1 \\ A_2 \end{pmatrix} = \left[-i\begin{pmatrix} \omega_1 & 0 \\ 0 & \omega_2 \end{pmatrix} - \begin{pmatrix} \gamma_1 & \gamma_{12} \\ \gamma_{12} & \gamma_2 \end{pmatrix} - \begin{pmatrix} \xi_1 & 0 \\ 0 & \xi_2 \end{pmatrix}\right]\begin{pmatrix} A_1 \\ A_2 \end{pmatrix} + \begin{pmatrix} \kappa_1 \\ \kappa_2 \end{pmatrix} s^+_{l,\sigma}, \tag{4}$$

where γ_j are radiative decay rates, ξ_j are absorptive decay rates, and κ_j are coupling coefficients to the incoming wave. Because both resonances radiate into the same channel $s^{\pm}_{l,\sigma}$, the radiative coupling rate γ_{12} is necessary to ensure energy conservation.[39] Absorptions do not have such constraints, so we let $\xi_{12} = 0$ for simplicity. Meanwhile, the outgoing wave is given by

$$s^-_{l,\sigma} = s^+_{l,\sigma} + d_1 A_1 + d_2 A_2, \tag{5}$$

where d_j are coupling coefficients, and the first term $s^-_{l,\sigma} = s^+_{l,\sigma}$ comes from the planewave itself.[1] Since we are considering nanostructures, we exclude the direct (non-resonant) background scattering process related to Fano resonances[34,35]; only the resonant scattering processes are considered here. The normalizations are chosen such that $|A_j|^2$ is the electromagnetic energy in each resonance and $|s^{\pm}_{l,\sigma}|^2$ is the incoming and outgoing power. For low absorption loss, we can apply energy conservation and time reversal symmetry[39] to eliminate many unknowns and get $\kappa_j = d_j$, $\gamma_j = -d_j^2/2$, and $\gamma_{12} = -d_1 d_2/2$. Solving Eqs 4 and 5 for a steady-state solution at frequency ω gives the reflection coefficient $s^-_{l,\sigma}/s^+_{l,\sigma}$ as

$$R_{l,\sigma} = 1 - 2\frac{\left[i(\omega_2 - \omega) + \xi_2\right]\gamma_1 + \left[i(\omega_1 - \omega) + \xi_1\right]\gamma_2}{\left[i(\omega_1 - \omega) + \gamma_1 + \xi_1\right]\left[i(\omega_2 - \omega) + \gamma_2 + \xi_2\right] - \gamma_1\gamma_2}, \tag{6}$$

which yields the scattering cross sections spectrum through Eq 2. When there is negligible absorption loss ($\xi_1 = \xi_2 = 0$), the particle becomes transparent in this channel ($R_{l,\sigma} = 1$) at

the "transparency frequency," defined as

$$\omega = \frac{\omega_1\gamma_2 + \omega_2\gamma_1}{\gamma_1 + \gamma_2} \equiv \omega_{\rm t}. \tag{7}$$

Since $\omega_{\rm t}$ is simply a weighted average of the two resonant frequencies, it *always* exists, regardless of the radiative decay rates and other system details. We therefore conclude that the scattering dark state is a general phenomenon in the low-absorption limit when two resonances in the same channel are simultaneously excited.

In the presence of material loss, the scattering cross section cannot be strictly zero even at $\omega_{\rm t}$. This can be viewed as a consequence of the optical theorem [1], which relates the forward scattering amplitude to the total extinction cross section (scattering plus absorption). Taking $\xi_1 = \xi_2 = \xi$ and $\gamma_1 = \gamma_2 = \gamma$, the reflection coefficient at $\omega_{\rm t}$ is $R_{l,\sigma} \approx 1 - 16\gamma\xi/(\omega_1 - \omega_2)^2$ to leading order of the absorptive decay rate ξ. So, the "low-absorption limit" can be quantified as $\xi \ll (\omega_1 - \omega_2)^2/\gamma$.

The scattering dark state occurs when the two outgoing waves d_1A_1 and d_2A_2 have equal magnitude and opposite phase, as illustrated in Figure 2b. When $\omega < \omega_1 < \omega_2$ or when $\omega > \omega_2 > \omega_1$, the two outgoing waves add up in phase (shown in blue dotted arrows). When $\omega_1 < \omega < \omega_2$, the two add up out of phase (shown in green dashed arrows). At the transparency frequency $\omega_{\rm t}$, the two waves exactly cancel each other (shown in red solid arrows), making the particle completely transparent in the (l, σ) channel.

We now address the choice of basis. In the derivation above, we choose a basis to express the two resonances such that $\omega_{12} = 0$ (no coupling in the absence of loss), and the scattering dark state arises from interference in the far-field radiation of the two resonances. The underlying system is independent of the basis, and we may as well choose a basis that diagonalizes the radiative-decay-rate matrix (so that $\gamma'_{12} = 0$, no radiative coupling; the

prime denotes variables in that basis); in such a basis, Eqs 4 and 5 become

$$\frac{d}{dt}\begin{pmatrix} A_1' \\ A_2' \end{pmatrix} = \left[-i \begin{pmatrix} \omega_1' & \omega_{12}' \\ \omega_{12}' & \omega_2' \end{pmatrix} - \begin{pmatrix} \gamma_1' & 0 \\ 0 & 0 \end{pmatrix} - \begin{pmatrix} \xi_1' & \xi_{12}' \\ \xi_{12}' & \xi_2' \end{pmatrix} \right] \begin{pmatrix} A_1' \\ A_2' \end{pmatrix} + \begin{pmatrix} \kappa_1' \\ 0 \end{pmatrix} s_{l,\sigma}^{+}, \qquad (8)$$

$$s_{l,\sigma}^{-} = s_{l,\sigma}^{+} + d_1' A_1',$$

with $\omega_1' = (\omega_1\gamma_1+\omega_2\gamma_2)/(\gamma_1+\gamma_2)$, $\omega_2' = (\omega_1\gamma_2+\omega_2\gamma_1)/(\gamma_1+\gamma_2)$, $\omega_{12}' = (\omega_2-\omega_1)\sqrt{\gamma_1\gamma_2}/(\gamma_1+\gamma_2)$, $\gamma_1' = \gamma_1 + \gamma_2$, and $\kappa_1' = d_1' = \sqrt{d_1^2 + d_2^2}$. The transformation of the absorptive decay rates is similar. We see that $\gamma_2' = 0$ (and so $\kappa_2' = d_2' = 0$). So, in this basis, resonance A_1' radiates, but resonance A_2' does not; this is exactly the subradiant-superradiant model[17,19,21,47,48]. Intuitively, this choice of basis is possible because there is only one channel of radiation, which can be incorporated into just one degree of freedom. The scattering dark state still exists in the low-absorption limit at the frequency given by Eq 7. But, now it is the direct near-field coupling ω_{12}' that leads to transparency. We therefore conclude that the scattering dark state can be interpreted as arising from the far-field coupling of two radiating resonances, or arising from the near-field coupling of one radiating resonance and a non-radiating resonance. Both interpretations are valid; it is only a matter of basis choice.

The extension to more than two resonances is described in Supporting Information. With n resonances in the same channel and with negligible absorption, scattering in this channel vanishes at frequencies given by

$$\sum_{j=1}^{n} \frac{\gamma_j}{\omega_j - \omega} = 0, \qquad (9)$$

where ω_j and γ_j are the resonant frequencies and radiative decay rates. The left-hand side swings from $-\infty$ to $+\infty$ in each interval between successive resonant frequencies. So, there is one transparency frequency in each of these $n-1$ intervals. For example, there is one transparency frequency with two resonances, two transparency frequencies with three resonances, *etc.* Similar to the two-resonance case, it is possible to choose a basis that diagonalizes the radiative-decay-rate matrix; in such a basis, one resonance radiates while

the other $n-1$ resonances do not—again, because there is only one channel of radiation.

This brings our major conclusion that the scattering dark state arises generally with multiple resonances in the same channel. It does not matter how many resonances there are, or how narrow or broad each resonance is. Therefore the suppressed scattering is more general than the discrete-coupled-to-continuum or narrow-coupled-to-broad scenarios in standard Fano resonances[33,34].

The scattering dark state is similar to "bound state in the continuum"[51–53] because both phenomena arise from destructive interference of outgoing waves. However, a scattering dark state is *not* a bound state. Eq 4 indicates that the resonance amplitudes decay to zero in the absence of the incoming wave—they cannot sustain oscillation on their own, even at the transparency frequency. Also, the particle becomes transparent at steady state, but at the transient stage when $d_1A_1 + d_2A_2 = 0$ has not been established, the particle is opaque.

Lastly, we provide a few explicit examples to illustrate the concepts discussed above. First, we consider a multi-layer sphere (schematically shown in the inset of Figure 3a) that consists of concentric metallic core, dielectric spacer, and metallic shell. For the first example, we describe the metal layers using the Drude model with negligible damping $\epsilon(\omega) = 1-\omega_{\rm p}^2/\omega^2$, let the dielectric layer be $\epsilon = 2.04$, and let the surrounding medium be air. For a particle of size $[r_1, r_2, r_3] = [0.005, 0.073, 0.132]\lambda_{\rm p}$ (where $\lambda_{\rm p} = 2\pi c/\omega_{\rm p}$ is the plasma wavelength, and c is the speed of light in vacuum), the exact scattering cross section is plotted as the black line in Figure 3a; these data are calculated using the Mie solution with the transfer matrix method.[54] The electric dipole channel TM_1 ($l = 1$, $\sigma = \mathrm{TM}$) dominates in the frequency range plotted; contributions from other channels are six orders of magnitude smaller. There is no absorption loss in this example, and as expected, the scattering cross section goes to zero at a transparency frequency $\omega_{\rm t}$ in between the two resonance peaks. We plot the steady-state electric-field profile at one of the resonant frequencies and at $\omega_{\rm t}$ in Figure 3b and 3c; animations of these field profiles are given in Supplementary Movies S1 and S2. The field profile confirms that the particle becomes invisible at $\omega_{\rm t}$. We note that the scattering dark

state is robust: perturbations of parameters (such as the layer thicknesses and the refractive indices) only shift the frequency where it occurs, consistent with our discussion above.

Figure 3a also shows the prediction from the temporal coupled-mode theory (red dashed line). We obtain the parameters in TCMT without doing curve fitting. Instead, we locate the two poles of the exact reflection coefficient $R_{1,\mathrm{TM}}$ (from the Mie solution) on the complex-frequency plane. The pole locations, $0.4411 - 0.00282i$ and $0.4456 - 0.00297i$ (in units of ω_p), yield the TCMT parameters $\omega_1 = 0.4397$, $\gamma_1 = 0.00285$, $\omega_2 = 0.4470$, and $\gamma_2 = 0.00294$ when compared to the denominator of Eq 6. The TCMT prediction agrees excellently with the exact Mie solution even without fitting.

A collection of these nanospheres with subwavelength spacing can act as an effective medium. In general, the scattering properties of such closely spaced nanospheres are substantially different from that of an individual nanosphere in free space. However, when an individual particle is transparent, we can use the superposition principle to conclude that a collection of particles is also transparent even when closed spaced. So, near ω_t, we may infer the properties of the effective medium from an individual particle in free space, using the standard mixing formula[55]. Near ω_t, the real part of the individual particle's electric polarizability changes rapidly (Figure 3d), so the refractive index n_eff of the effective medium changes rapidly. This leads to a suppressed group velocity, $v_\mathrm{g} = d\omega/dk = c/(n_\mathrm{eff} + \omega dn_\mathrm{eff}/d\omega)$, for a wave packet propagating through this medium, analogous to the atomic version of electromagnetically induced transparency[56,57] and similar to the metamaterial realization using subwavelength optical antennas[46–48]. For example, for a random collection of the above-mentioned particles with concentration $N = (\lambda_\mathrm{t}/3)^{-3}$ (where $\lambda_\mathrm{t} = 2\pi c/\omega_\mathrm{t}$ is the transparency wavelength), the group velocity is $v_\mathrm{g} \approx c/200$ at transparency.

Next, we provide examples using realistic materials with loss. Consider the same multilayer sphere schematically shown in the inset of Figure 3a, but with the metal layers being silver (complex permittivity from experimental data[58]) instead. Similar metal-dielectric-metal nanospheres have been synthesized[17,59] and studied numerically[54,60–63] in prior works.

To mimic potential experimental condition, we consider such nanospheres suspended in an aqueous solution ($\epsilon = 1.77$). Figure 4a shows the exact scattering cross section for a particle of size $[r_1, r_2, r_3] = [20, 31, 52]$ nm. This particle is large enough that the electrostatic approximation is not appropriate, but small enough that the TM_1 channel dominates. Since the absorption and radiation loss is relatively large, the prediction from TCMT is not as accurate in this example; nonetheless, we still observe a clear dip in the scattering cross section that is suppressed by more than a factor of ten compared to the on-resonance values. Supplementary Movies S3 and S4 show animations of the field propagation on-resonance and at the almost-transparent wavelength, where the particle becomes almost invisible. Such nanoparticles can be useful for the application of transparent projection screens using resonant scattering of nanoparticles.[64] In the presence of absorption loss, the amount of scattering at ω_t does vary with perturbations. As discussed earlier, $R_{l,\sigma} \approx 1 - 16\gamma\xi/(\omega_1 - \omega_2)^2$ depends on the absorptive loss, radiative loss, and the frequency difference between the two resonances. However, the dip still exists with reasonable perturbations: for the current structure, the scattering minimum remains at least 10 times smaller than the scattering maximum with a 10% change in any thickness or refractive index parameter.

Another possible application of the scattering dark state is to selectively allow only a narrow bandwidth of light to pass through a medium. In a medium with dilute suspension of particles, the transmission is given by the Beer-Lambert law $T = \exp(-\sigma_{\text{ext}} N l)$, where $\sigma_{\text{ext}} = \sigma_{\text{sca}} + \sigma_{\text{abs}}$ is the extinction cross section of an individual particle, N is its number density, and l is the path length of the medium. Typically, resonant nanoparticles suppress transmission at a target wavelength. But with the scattering dark state, we may enhance transmission at a target wavelength instead. Figure 4b shows one example using the same type of silver-silica-silver nanosphere, designed to allow light with wavelength around 600 nm to pass through.

Our theory derivation suggests that the scattering dark state is not limited to any particular type of resonance; nor is it limited to any particular radiation channel. To illustrate

these points, we consider a purely dielectric nanostructure that supports whispering-gallery resonances in multiple angular momentum channels. Specifically, we consider a nanosphere consisting of four concentric layers that alternate between a high-index dielectric ($\epsilon = 12$, can be silicon or gallium arsenide) and a low-index dielectric ($\epsilon = 1$, can be a transparent aerogel[65]). For a particle of size $[r_1, r_2, r_3, r_4] = [40, 90, 150, 160]$ nm, Figure 5 shows the exact scattering cross section divided into individual channels as in Eq 2. Scattering dark states can be seen in the TE_1, TE_2, and TE_3 channels. Note that due to the spectral overlap of the different channels, the particle may become transparent to one particular channel but not the rest; in principle, it is possible to probe the individual channels by preparing special excitation waves (for example, a tightly-focused beam can isolate the dipole channels[66]).

In summary, we have presented an analytical treatment for the general problem of light scattering from a multi-resonant nanostructure that is spherical or non-spherical but sub-wavelength in size. With n resonances in the same channel, $n-1$ scattering dark states arise when the absorption loss is negligible; this result is independent of the radiative decay rates and many other system details. The scattering dark state can be interpreted as arising from far-field or near-field coupling, depending on the choice of basis. This theoretical treatment should improve the understanding of scattering dark states and provide guidance for future works on this topic.

It will be interesting to consider perturbations that break the spherical symmetry of the scatterer, allowing each resonance to couple to multiple channels. The interference between multiple resonances in multiple channels may lead to even richer phenomena[11,17,39,67].

Acknowledgement

The authors thank Owen Miller, Bo Zhen, Hongsheng Chen, and Ruixun Zhang for helpful discussions. This work was partially supported by the Army Research Office through the Institute for Soldier Nanotechnologies under Contract No. W911NF-13-D-0001, and also in part by the Materials Research Science and Engineering Centers of the National Science

Foundation under grant No. DMR-0819762.

Supporting Information Available

Scattering dark states with arbitrarily many resonances in the same channel (Supplementary Text); animations of the field propagation for the lossless metal-dielectric-metal nanosphere (Supplementary Movies S1 and S2) and for the silver-silica-silver example with loss (Supplementary Movies S3 and S4). This material is available free of charge via the Internet at `http://pubs.acs.org/`.

Author Information

The authors declare no competing financial interest.

References

(1) Bohren, C. F.; Huffman, D. R. *Absorption and Scattering of Light by Small Particles*; Wiley: New York, 1998.

(2) Hamam, R. E.; Karalis, A.; Joannopoulos, J. D.; Soljačić, M. *Phys. Rev. A* **2007**, *75*, 053801.

(3) Ruan, Z.; Fan, S. *Appl. Phys. Lett.* **2011**, *98*, 043101.

(4) Prodan, E.; Radloff, C.; Halas, N. J.; Nordlander, P. *Science* **2003**, *302*, 419–422.

(5) Miroshnichenko, A. E.; Flach, S.; Kivshar, Y. S. *Rev. Mod. Phys.* **2010**, *82*, 2257–2298.

(6) Luk'yanchuk, B.; Zheludev, N. I.; Maier, S. A.; Halas, N. J.; Nordlander, P.; Giessen, H.; Chong, C. T. *Nature Mater.* **2010**, *9*, 707–715.

(7) Rahmani, M.; Luk'yanchuk, B.; Hong, M. *Laser Photonics Rev.* **2013**, *7*, 329–349.

(8) Khanikaev, A. B.; Wu, C.; Shvets, G. *Nanophotonics* **2013**, *2*, 247–264.

(9) Halas, N. J.; Lal, S.; Chang, W.-S.; Link, S.; Nordlander, P. *Chem. Rev.* **2011**, *111*, 3913–3961.

(10) Verellen, N.; Sonnefraud, Y.; Sobhani, H.; Hao, F.; Moshchalkov, V. V.; Dorpe, P. V.; Nordlander, P.; Maier, S. A. *Nano Lett.* **2009**, *9*, 1663–1667.

(11) Sonnefraud, Y.; Verellen, N.; Sobhani, H.; Vandenbosch, G. A.; Moshchalkov, V. V.; Van Dorpe, P.; Nordlander, P.; Maier, S. A. *ACS Nano* **2010**, *4*, 1664–1670.

(12) Artar, A.; Yanik, A. A.; Altug, H. *Nano Lett.* **2011**, *11*, 1685–1689.

(13) Giannini, V.; Francescato, Y.; Amrania, H.; Phillips, C. C.; Maier, S. A. *Nano Lett.* **2011**, *11*, 2835–2840.

(14) Gallinet, B.; Martin, O. J. F. *Phys. Rev. B* **2011**, *83*, 235427.

(15) Gallinet, B.; Martin, O. J. F. *ACS Nano* **2011**, *5*, 8999–9008.

(16) Rahmani, M.; Lei, D. Y.; Giannini, V.; Lukiyanchuk, B.; Ranjbar, M.; Liew, T. Y. F.; Hong, M.; Maier, S. A. *Nano Lett.* **2012**, *12*, 2101–2106.

(17) Mukherjee, S.; Sobhani, H.; Lassiter, J. B.; Bardhan, R.; Nordlander, P.; Halas, N. J. *Nano Lett.* **2010**, *10*, 2694–2701.

(18) Artar, A.; Yanik, A. A.; Altug, H. *Nano Lett.* **2011**, *11*, 3694–3700.

(19) Lassiter, J. B.; Sobhani, H.; Knight, M. W.; Mielczarek, W. S.; Nordlander, P.; Halas, N. J. *Nano Lett.* **2012**, *12*, 1058–1062.

(20) Lovera, A.; Gallinet, B.; Nordlander, P.; Martin, O. J. *ACS Nano* **2013**, *7*, 4527–4536.

(21) Adato, R.; Artar, A.; Erramilli, S.; Altug, H. *Nano Lett.* **2013**, *13*, 2584–2591.

(22) Davis, T. J.; Gómez, D. E.; Vernon, K. C. *Nano Lett.* **2010**, *10*, 2618–2625.

(23) Forestiere, C.; Dal Negro, L.; Miano, G. *Phys. Rev. B* **2013**, *88*, 155411.

(24) Kometani, N.; Tsubonishi, M.; Fujita, T.; Asami, K.; Yonezawa, Y. *Langmuir* **2001**, *17*, 578–580.

(25) Wiederrecht, G. P.; Wurtz, G. A.; Hranisavljevic, J. *Nano Lett.* **2004**, *4*, 2121–2125.

(26) Fofang, N. T.; Park, T.-H.; Neumann, O.; Mirin, N. A.; Nordlander, P.; Halas, N. J. *Nano Lett.* **2008**, *8*, 3481–3487.

(27) Wu, X.; Gray, S. K.; Pelton, M. *Opt. Express* **2010**, *18*, 23633–23645.

(28) Manjavacas, A.; Abajo, F. J. G. d.; Nordlander, P. *Nano Lett.* **2011**, *11*, 2318–2323.

(29) Schlather, A. E.; Large, N.; Urban, A. S.; Nordlander, P.; Halas, N. J. *Nano Lett.* **2013**, *13*, 3281–3286.

(30) Zengin, G.; Johansson, G.; Johansson, P.; Antosiewicz, T. J.; Käll, M.; Shegai, T. *Sci. Rep.* **2013**, *3*, 3074.

(31) Cao, L.; Fan, P.; Brongersma, M. L. *Nano Lett.* **2011**, *11*, 1463–1468.

(32) Kim, S.-K.; Day, R. W.; Cahoon, J. F.; Kempa, T. J.; Song, K.-D.; Park, H.-G.; Lieber, C. M. *Nano Lett.* **2012**, *12*, 4971–4976.

(33) Fano, U. *Phys. Rev.* **1961**, *124*, 1866–1878.

(34) Ruan, Z.; Fan, S. *J. Phys. Chem. C* **2010**, *114*, 7324–7329.

(35) Ruan, Z.; Fan, S. *Phys. Rev. A* **2012**, *85*, 043828.

(36) Garrido Alzar, C. L.; Martinez, M. A. G.; Nussenzveig, P. *Am. J. Phys.* **2002**, *70*, 37–41.

(37) Joe, Y. S.; Satanin, A. M.; Kim, C. S. *Phys. Scr.* **2006**, *74*, 259.

(38) Opatrný, T.; Welsch, D.-G. *Phys. Rev. A* **2001**, *64*, 023805.

(39) Suh, W.; Wang, Z.; Fan, S. *IEEE J. Quantum Electron.* **2004**, *40*, 1511–1518.

(40) Smith, D. D.; Chang, H.; Fuller, K. A.; Rosenberger, A. T.; Boyd, R. W. *Phys. Rev. A* **2004**, *69*, 063804.

(41) Maleki, L.; Matsko, A. B.; Savchenkov, A. A.; Ilchenko, V. S. *Opt. Lett.* **2004**, *29*, 626–628.

(42) Naweed, A.; Farca, G.; Shopova, S. I.; Rosenberger, A. T. *Phys. Rev. A* **2005**, *71*, 043804.

(43) Xu, Q.; Sandhu, S.; Povinelli, M. L.; Shakya, J.; Fan, S.; Lipson, M. *Phys. Rev. Lett.* **2006**, *96*, 123901.

(44) Tomita, M.; Totsuka, K.; Hanamura, R.; Matsumoto, T. *J. Opt. Soc. Am. B* **2009**, *26*, 813–818.

(45) Fedotov, V. A.; Rose, M.; Prosvirnin, S. L.; Papasimakis, N.; Zheludev, N. I. *Phys. Rev. Lett.* **2007**, *99*, 147401.

(46) Papasimakis, N.; Fedotov, V. A.; Zheludev, N. I.; Prosvirnin, S. L. *Phys. Rev. Lett.* **2008**, *101*, 253903.

(47) Zhang, S.; Genov, D. A.; Wang, Y.; Liu, M.; Zhang, X. *Phys. Rev. Lett.* **2008**, *101*, 047401.

(48) Liu, N.; Langguth, L.; Weiss, T.; Kästel, J.; Fleischhauer, M.; Pfau, T.; Giessen, H. *Nature Mater.* **2009**, *8*, 758–762.

(49) Tribelsky, M. I.; Flach, S.; Miroshnichenko, A. E.; Gorbach, A. V.; Kivshar, Y. S. *Phys. Rev. Lett.* **2008**, *100*, 043903.

(50) Haus, H. A. *Waves and Fields in Optoelectronics*; Prentice Hall: Englewood Cliffs, NJ, 1984.

(51) Marinica, D. C.; Borisov, A. G.; Shabanov, S. V. *Phys. Rev. Lett.* **2008**, *100*, 183902.

(52) Hsu, C. W.; Zhen, B.; Chua, S.-L.; Johnson, S. G.; Joannopoulos, J. D.; Soljačić, M. *Light: Science & Applications* **2013**, *2*, e84.

(53) Hsu, C. W.; Zhen, B.; Lee, J.; Chua, S.-L.; Johnson, S. G.; Joannopoulos, J. D.; Soljačić, M. *Nature* **2013**, *499*, 188–191.

(54) Qiu, W.; DeLacy, B. G.; Johnson, S. G.; Joannopoulos, J. D.; Soljačić, M. *Opt. Express* **2012**, *20*, 18494–18504.

(55) Sihvola, A. H. *Electromagnetic mixing formulas and applications*; Institution of Electrical Engineers: London, 1999.

(56) Harris, S. E. *Phys. Today* **1997**, *50*, 36.

(57) Hau, L. V.; Harris, S. E.; Dutton, Z.; Behroozi, C. H. *Nature* **1999**, *397*, 594–598.

(58) Palik, E. D. *Handbook of Optical Constants of Solids*; Academic Press: New York, 1985.

(59) Bardhan, R.; Mukherjee, S.; Mirin, N. A.; Levit, S. D.; Nordlander, P.; Halas, N. J. *J. Phys. Chem. C* **2010**, *114*, 7378–7383.

(60) Wang, M.; Cao, M.; Chen, X.; Gu, N. *J. Phys. Chem. C* **2011**, *115*, 20920–20925.

(61) Wu, D.; Jiang, S.; Liu, X. *J. Phys. Chem. C* **2011**, *115*, 23797–23801.

(62) Ho, J. F.; Luk'yanchuk, B.; Zhang, J. B. *Appl. Phys. A: Mater. Sci. Process.* **2012**, *107*, 133–137.

(63) Sikdar, D.; Rukhlenko, I. D.; Cheng, W.; Premaratne, M. *J. Opt. Soc. Am. B* **2013**, *30*, 2066–2074.

(64) Hsu, C. W.; Zhen, B.; Qiu, W.; Shapira, O.; DeLacy, B. G.; Joannopoulos, J. D.; Soljačić, M. *Nat. Commun.* **2014**, *5*, 3152.

(65) Tabata, M.; Adachi, I.; Kawai, H.; Kubo, M.; Sato, T. *Phys. Procedia* **2012**, *37*, 642–649.

(66) Mojarad, N. M.; Sandoghdar, V.; Agio, M. *J. Opt. Soc. Am. B* **2008**, *25*, 651–658.

(67) Wang, H.; Wu, Y.; Lassiter, B.; Nehl, C. L.; Hafner, J. H.; Nordlander, P.; Halas, N. J. *Proc. Natl. Acad. Sci. U.S.A.* **2006**, *103*, 10856–10860.

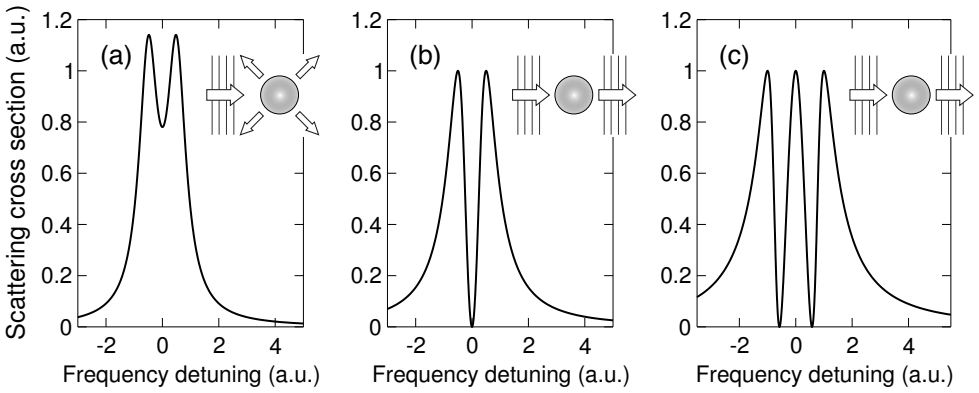

Figure 1: Schematic plots for light scattering when multiple resonances are excited simultaneously. (a) Two resonances in different radiation channels (*e.g.*, TM_1 and TE_1). In this case, radiation from the two resonances add up incoherently, and the cross section is a sum of two Lorentzian functions. The particle is opaque in between the two resonances (illustrated in the inset). (b) Two resonances in the same radiation channel. In this case, radiation from the two resonances add up coherently, giving rise to a different line shape and a scattering dark state where the particle becomes transparent (illustrated in the inset). (c) Three resonances in the same radiation channel. Here, two scattering dark states arise (illustrated in the inset).

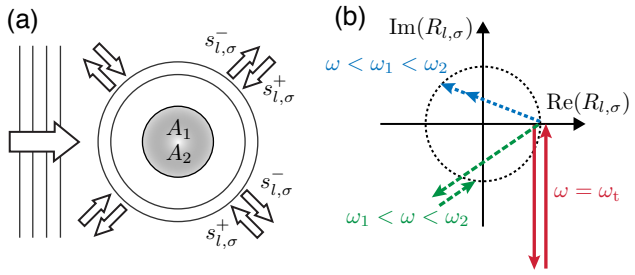

Figure 2: Illustration of a scattering dark state in a doubly resonant nanostructure. (a) Abstract diagram showing a nanostructure where two resonances, A_1 and A_2, in the same angular momentum l and polarization σ channel are simultaneously excited by incoming wave $s^+_{l,\sigma}$, and both radiate into outgoing wave $s^-_{l,\sigma}$. (b) Schematic illustrations showing the complex reflection coefficient $R_{l,\sigma} = s^-_{l,\sigma}/s^+_{l,\sigma}$ with contributions from the two resonances (each indicated by an arrow). When absorption loss is negligible, $R_{l,\sigma}$ always lands on the unit circle, and the two outgoing waves add up either in phase or out of phase. Different excitation frequencies are shown by arrows of different colors; at frequency ω_t, the two outgoing waves cancel, giving rise to a scattering dark state where the particle becomes transparent.

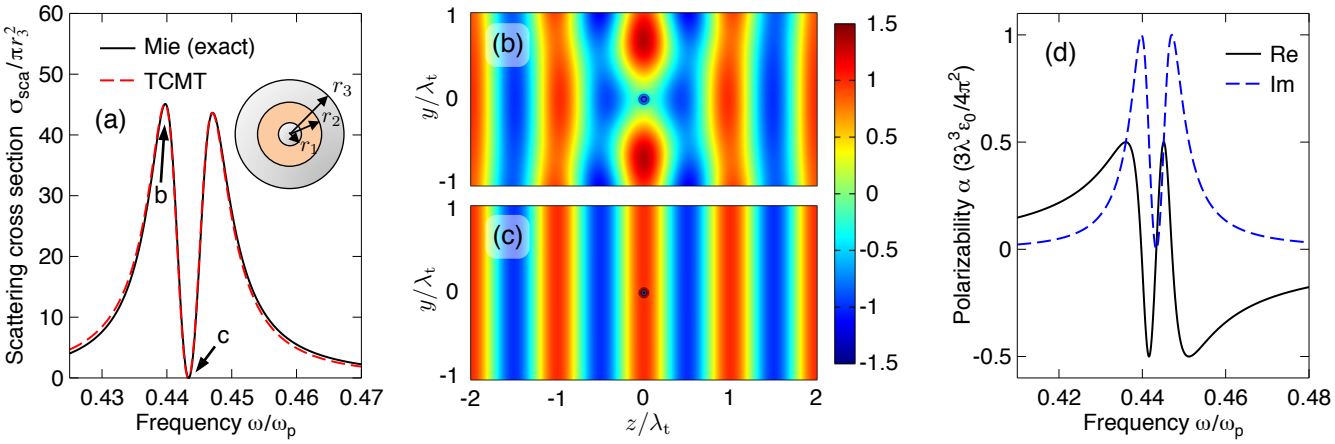

Figure 3: Scattering dark state in a doubly resonant nanosphere without absorption loss. (a) The particle's scattering cross section in air, calculated by the Mie solution (black solid line) and the temporal coupled-mode theory (red dashed line). The inset schematically shows the particle's composition: concentric metallic core, silica spacer ($\epsilon = 2.04$), and metallic shell, with radii $[r_1, r_2, r_3] = [0.005, 0.073, 0.132]\lambda_p$. The metal is described by the Drude model with plasma frequency ω_p and negligible damping. In the plotted range of frequency, the cross section is dominated by the TM_1 channel (electric dipole). (b, c) Steady-state electric-field pattern, $\mathrm{Re}(E_x)$, with an incident wave $\mathbf{E}_{inc} = e^{ikz}\hat{\mathbf{x}}$ that is (b) at the resonant frequency ω_1 and (c) at the transparency frequency ω_t. Animations of the field propagation are shown in Supplementary Movies S1 and S2. (d) Electric polarizability of this particle in air. At the transparency frequency, the large slope of $\mathrm{Re}(\alpha)$ can give rise to slow group velocity for a wave packet propagating through a collection of such particles.

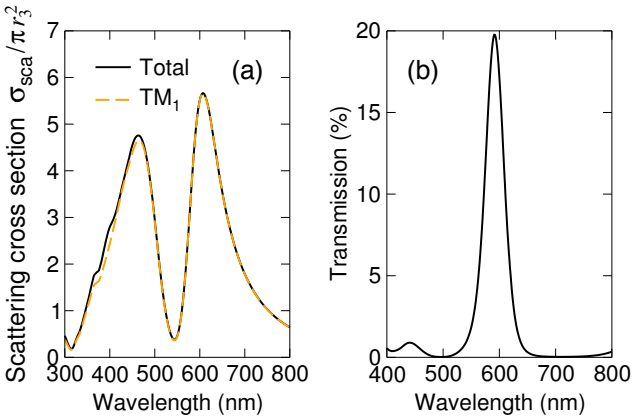

Figure 4: Scattering dark state in a doubly resonant nanosphere with absorption loss. (a) The scattering cross section of a particle consisting of concentric silver core, silica spacer ($\epsilon = 2.04$), and silver shell, with radii of the layers being $[r_1, r_2, r_3] = [20, 31, 52]$ nm. The cross section is calculated with the Mie solution with the particle in water ($\epsilon = 1.77$) and the complex permittivity of silver taken from experimental data.[58] Solid line shows the sum from all channels, and dashed line shows the contribution from the TM$_1$ channel. Animations of the field propagation at 607 nm and 544 nm are shown in Supplementary Movies S3 and S4. (b) Transmission spectrum for a dilute aqueous solution of nanoparticles of size $[r_1, r_2, r_3] = [33, 55, 77]$ nm, with the number density times path length being 7×10^9 cm^{-2}.

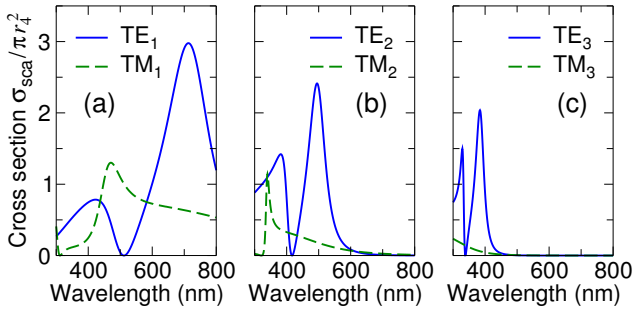

Figure 5: Scattering dark states in individual channels of a nanosphere made of dielectrics only. The particle consists of four concentric layers, with relative permittivities being $[\epsilon_1, \epsilon_2, \epsilon_3, \epsilon_4] = [1, 12, 1, 12]$ and radii being $[r_1, r_2, r_3, r_4] = [40, 90, 150, 160]$ nm. (a)-(c) The particle's scattering cross section in air, separated into different angular momentum and polarization channels. Scattering dark states can be seen in the TE$_1$, TE$_2$, and TE$_3$ channels.

For TOC Only

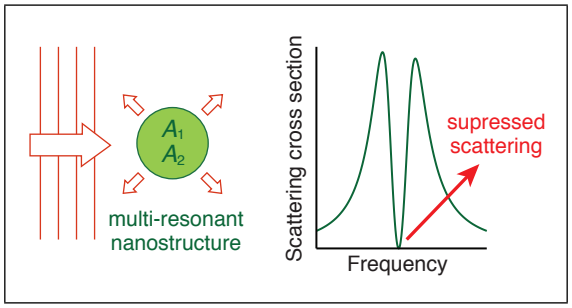
A1
A2
multi-resonant
nanostructure
Scattering cross section
Frequency
supressed
scattering

Supporting Information

Theoretical criteria for scattering dark states in nanostructured particles

Chia Wei Hsu,[1,2] Brendan G. DeLacy,[3] Steven G. Johnson,[4] John D. Joannopoulos,[1] and Marin Soljačić[1]

[1]*Department of Physics, Massachusetts Institute of Technology, Cambridge, MA 02139, USA.*
[2]*Department of Physics, Harvard University, Cambridge, MA 02138, USA.*
[3]*U.S. Army Edgewood Chemical Biological Center, Aberdeen Proving Ground, MD 21010, USA.*
[4]*Department of Mathematics, Massachusetts Institute of Technology, Cambridge, MA 02139, USA.*

Arbitrarily many resonances in the same channel

In the main text, we consider the case of two spectrally overlapping resonances in the same channel. Here, we consider the more general case with arbitrarily many overlapping resonances in channel (l,σ). The temporal coupled-mode theory equations is now written in matrix form:

$$\begin{aligned}\frac{dA}{dt} &= (-i\Omega - \Gamma - \Xi)\, A + K^{\mathrm{T}} s^{+}_{l,\sigma},\\ s^{-}_{l,\sigma} &= s^{+}_{l,\sigma} + DA.\end{aligned} \tag{S.1}$$

Similar to the two-resonance case, we choose the basis such that Ω is diagonal (so that the resonances are orthogonal when we take the loss to zero), and we ignore any direct (non-resonant) background scattering process. With n resonances, the matrices are

$$A = \begin{pmatrix} A_1 \\ A_2 \\ \vdots \\ A_n \end{pmatrix}, \quad \Omega = \begin{pmatrix} \omega_1 & 0 & \dots & 0 \\ 0 & \omega_2 & \dots & 0 \\ \vdots & \vdots & \ddots & \vdots \\ 0 & 0 & \dots & \omega_n \end{pmatrix}, \quad \Gamma = \begin{pmatrix} \gamma_1 & \gamma_{12} & \dots & \gamma_{1n} \\ \gamma_{21} & \gamma_2 & \dots & \gamma_{2n} \\ \vdots & \vdots & \ddots & \vdots \\ \gamma_{n1} & \gamma_{n2} & \dots & \gamma_n \end{pmatrix}, \quad \Xi = \begin{pmatrix} \xi_1 & \xi_{12} & \dots & \xi_{1n} \\ \xi_{21} & \xi_2 & \dots & \xi_{2n} \\ \vdots & \vdots & \ddots & \vdots \\ \xi_{n1} & \xi_{n2} & \dots & \xi_n \end{pmatrix}, \tag{S.2}$$
$$K = \begin{pmatrix} \kappa_1, & \kappa_2, & \dots & \kappa_n \end{pmatrix}, \quad D = \begin{pmatrix} d_1, & d_2, & \dots & d_n \end{pmatrix}.$$

The meaning of these variables are the same as Eqs. (4) and (5) in the main text. With incoming light at frequency ω, Eq. (S.1) gives the steady-state reflection coefficient $s^{-}_{l,\sigma}/s^{+}_{l,\sigma}$ as

$$R_{l,\sigma} = 1 + D\left[i(\Omega - \omega I_n) + \Gamma + \Xi\right]^{-1} K^{\mathrm{T}}, \tag{S.3}$$

where I_n is the n-by-n identity matrix. The particle becomes transparent in this channel when $R_{l,\sigma} = 1$. Optical theorem suggests that zero scattering can only occur with zero absorption; therefore, we consider the small-absorption limit, $\Xi = 0$. Energy conservation and time reversal symmetry require the matrices to satisfy $K = D$, $D^{\dagger}D = 2\Gamma$, and $D^{*} = -D$, as shown in ref 39. Therefore, the transparency condition can be simplified to

$$D\left[i(\Omega - \omega I_n) - \frac{1}{2} D^{\mathrm{T}} D\right]^{-1} D^{\mathrm{T}} = 0. \tag{S.4}$$

By rewriting the matrix inverse using the Woodbury matrix identity, we see that this condition is satisfied when $D(\Omega - \omega I_n)^{-1} D^{\mathrm{T}} = 0$, which can be written as

$$\sum_{j=1}^{n} \frac{\gamma_j}{\omega_j - \omega} = 0 \tag{S.5}$$

because $d_j^2 = -2\gamma_j$. This is Eq. (11) in the main text. This simple expression yields all the transparency frequencies. We can immediately observe that, as we gradually increase ω, the left-hand side of Eq. (S.5) swings from $-\infty$ to $+\infty$ in each interval between successive resonant frequencies. So, there is one transparency frequency in each of these $n-1$ intervals. For example, there is one transparency frequency with two resonances, two transparency frequencies with three resonances, *etc.*

Similar to the two-resonance case, it is possible to choose a basis that diagonalizes the radiative-decay-rate matrix Γ. The matrix $\Gamma = -\frac{1}{2} D^{\mathrm{T}} D$ is a rank-one matrix, so only one of its n eigenvalues is non-zero. This non-zero eigenvalue is $-\frac{1}{2}\sum_{j=1}^{n} d_j^2 = \sum_{j=1}^{n} \gamma_j$. Therefore, in the basis where Γ is diagonal, one resonance would radiate while the other $n-1$ resonances do not. Intuitively, this is because there is only one channel of radiation.